ADVANCED FUNCTIONAL MATERIALS
www.afm-journal.de

Perfluorinated Ionomer-Modified Hole-Injection Layers: Ultrahigh-Workfunction but Nonohmic Contacts

Dagmawi Belaineh, Jun-Kai Tan, Rui-Qi Png, Pei-Fang Dee, Yi-Min Lee, Bao-Nguyen Nguyen Thi, Nur-Sabrina Ridzuan, and Peter K. H. Ho*

Recently it has been reported that Nafion oligomers, i.e., 2-(2-sulfonatotetrafluoroethoxy)-2-trifluoromethyltrifluoroethoxyfunctionalized oligotetrafluoroethylenes, also called perfluorinated ionomers (PFIs), can be blended into poly(3,4-ethylenedioxythiophene):poly(styrenesulfonic acid) (PEDT:PSSH) films to increase their workfunctions beyond 5.2 eV. These PFI-modified films are useful for energy-level alignment studies, and have been proposed as hole-injection layers (HILs). It is shown here however that these HILs do not provide sufficiently fast hole transfer into adjacent polymer semiconductor layers with ionization potentials deeper than ≈5.2 eV. X-ray and ultraviolet photoemission spectroscopies reveal that these HILs exhibit a molecularly-thin PFI overlayer that sets up a surface dipole that provides the ultrahigh workfunction. This dipolar layer persists even when the subsequent organic semiconductor layer is deposited, as evidenced by measurements of the diode built-in potentials. As a consequence, the PFI-modified HILs produce a higher contact resistance, and a lower equilibrium density of holes at the semiconductor contact than might have been expected from simple thermodynamic considerations of the reduction in hole-injection barrier. Thus the use of insulating dipolar surface layers at the charge-injection contact to tune its workfunction to match the relevant transport level of the semiconductor is of limited utility to achieve ohmic contact in these devices.

1. Introduction

An ohmic contact to an undoped semiconductor is one that can furnish a sufficiently large carrier density to the semiconductor side of the contact to provide a space-charge-limited-current (SCLC) density through the semiconductor. This depends on the current density demanded through the semiconductor. For an SCLC current density $J_{SCLC} \approx 100$ mA cm^{-2} through an organic semiconductor (OSC) diode, which corresponds to typical operating conditions, the rate of carriers that has to be supplied through the contact is 6×10^{17} cm^{-2} s^{-1}. An ohmic contact has to be able to deliver this injection rate without requiring a macroscopic electric field at the contact. Achieving ohmic contacts is the key to maximizing the power efficiency of OSC devices, including organic light-emitting diodes, field-effect transistors, and solar cells, and improving their operational stability. However the criteria for ohmic contacts in OSC devices are still under investigation.[1–3]

A well-known way to achieve ohmic hole contacts is to use electrodes with high workfunctions. This reduces the thermodynamic barrier for hole injection Δ_h given by $\Delta_h = I_{p,OSC} - \phi_{el}$, where I_p is the ionization potential of the OSC, measured at the edge of the highest-occupied-molecular-orbital (HOMO) band, and ϕ_{el} is the effective workfunction of the hole-injecting electrode inside the device.[4] This effective workfunction may differ from its vacuum workfunction ϕ_{vac} that is conventionally measured by ultraviolet photoemission spectroscopy (UPS), due to effects that shift the vacuum level (VL; the energy of this level denoted E_{vac}) across the contact, including Fermi-level (E_F) pinning.[5,6] The effective $I_{p,OSC}$ may also be reduced at the contact by polarization-induced band-bending.[7–9] Thus the required ϕ_{vac} to achieve ohmic hole contact to an OSC with a given I_p depends also on the details of the contact. For the case of weakly interacting contacts where ϕ_{el} deviates from ϕ_{vac} only through charge-transfer E_F pinning, which appears to be the usual case for OSCs in contact with *p*-doped semiconducting polymer electrodes, a rule-of-thumb suggests ϕ_{vac} of the electrode needs to approach within 0.2 eV of, or exceed, the I_p of the OSC.[10]

When this condition is met, the OSC side of the contact exhibits a significant hole-carrier density due to charge-transfer doping from the adjacent electrode that equalizes E_F.[11] This hole density forms an ultrathin carrier sheet, only a few nanometers thick, which we labeled the δ-doped layer, whose carrier density can be estimated through subgap charge-modulation spectroscopy during the usual electroabsorption (EA) spectroscopy of OSC diodes.[10,12] The thickness-integrated hole density in this layer is called the δ-hole density. Detailed measurements using PEDT:PSSM electrodes, where M refers to spectator cations used to tune ϕ_{vac} of the hole-injection layer (HIL), suggest that a minimum δ-hole density is required of the order of a few 10^{11} cm^{-2} to obtain ohmic contacts to typical polymer

Dr. D. Belaineh, J.-K. Tan, Dr. R.-Q. Png, P.-F. Dee, Y.-M. Lee, B.-N. N. Thi, N.-S. Ridzuan, Prof. P. K. H. Ho
Department of Physics
National University of Singapore
Lower Kent Ridge Road, S117550, Singapore
E-mail: phypngrq@nus.edu.sg

DOI: 10.1002/adfm.201500784

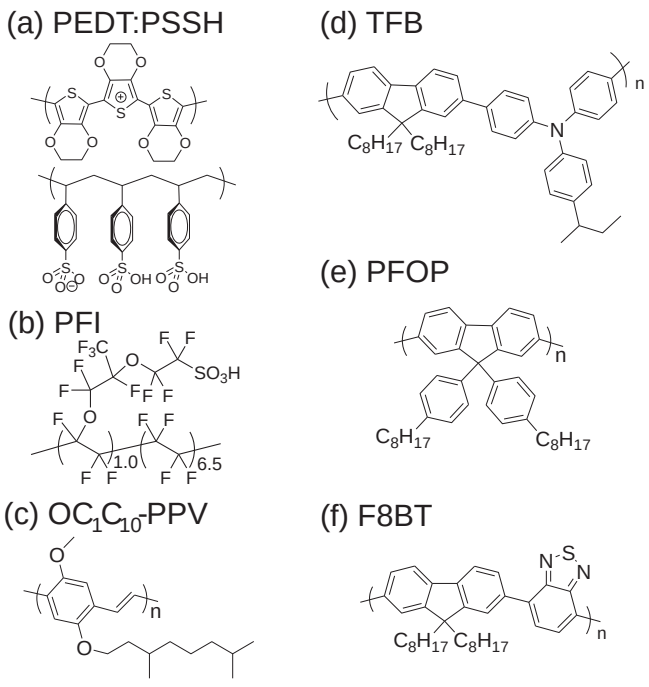

Figure 1. Chemical structures of materials used in this study: a) PEDT:PSSH, b) PFI, c) OC_1C_{10}-PPV, d) TFB, e) PFOP, and f) F8BT.

OSC films.[10,12] This indicates that heavy doping of the contact, by charge transfer or otherwise, may be more fundamental to achieving an ohmic contact, reminiscent of that in inorganic semiconductor devices. Furthermore it is clear that the hole-injection contact needs to be able to provide sufficiently fast hole injection to maintain this contact hole density to supply the SCLC. These aspects have often been neglected in the literature.

With the current industry effort migrating toward deeper-I_p OSCs for better stability and easier electron injection, it is a pressing goal to develop better hole injectors which can make ohmic hole contacts to these OSCs. Recently, it was reported that perfluorinated ionomers (PFIs) (chemical structure in **Figure 1**)[13] can be blended into well-established HILs, such as PEDT:PSSH[14,15] and sulfonated poly(thiophene-3-[2-(2-methoxyethoxy)ethoxy]-2,5-diyl):poly(4-hydroxystyrene) (S-P3MEET:PHOST),[16,17] to significantly enhance their ϕ_{vac} from 5.0–5.2 eV to 5.6–5.7 eV.[18–22] An improvement in the current density–voltage (*JV*) characteristics of some test diodes fabricated with these PFI-modified HILs has been reported. [19–22] However little is known about the surface composition and electronic properties of these modified blends, other than they are surface-enriched with PFI which appears responsible for the large ϕ_{vac}.[19,20] Curiously the reported improvement in *JV* characteristics has been modest for deep-I_p OSCs,[19–22] far short of the performance of ohmic contacts that can be generated for example by chemical doping of the OSC interlayer at the contact.[23] In addition, an electron-blocking mechanism may also have contributed to or even dominated the characteristics of the double-carrier diodes used in those reports, analogous to what is observed when a semiconducting or insulating monolayer is assembled at the hole-injection contact.[24,25]

In this work, we identified the origin of the increased work-function of the PFI-modified HILs and clarified the limitations in making ohmic hole contacts with this approach. These are two long-standing puzzles that have not adequately been addressed in the literature. We studied the PEDT:PSSH:PFI system as a model for ultrahigh-workfunction electrodes created through a dipolar dielectric surface layer, an approach that is of widespread current interest. The insights gained here may thus be relevant also to other methods using self-assembled monolayers,[26–28] dielectric polyelectrolytes, and amine-functionalized dielectric polymers.[29] We show here that the ultrahigh workfunction in the PEDT:PSSH:PFI system is generated by a VL shift through the frontier insulating monolayer of the HILs, rather than an electrochemical shift of E_F of their hole carriers. As a result, the E_F of the HIL can more closely approach the HOMO edge of a deep-I_p OSC, decreasing the apparent Δ_h, but does not provide a sufficient carrier density to the contact to turn it ohmic. Thus the PEDT:PSSH:PFI HILs perform only a little better than PEDT:PSSH as a hole injector into a variety of polymer OSCs.

2. Results and Discussion

Figure 1 shows the chemical structures of the materials used in this work. The commercial PEDT:PSSH solution contains *p*-doped PEDT chains dispersed in poly(styrenesulfonic acid)[14] and often contains metallic ion and other impurities. In this work, PEDT:PSSH and PSSH solutions were first purified by dialysis with semiconductor-grade hydrochloric acid (0.1 M) followed by Millipore water.[30] This procedure is important to remove free ions, and the sulfuric acid by-product of PSSH desulfonation. PEDT:PSSH solutions with different volume fractions of PEDT and PSSH were then prepared by combining the purified PEDT:PSSH and PSSH solutions to give formulations containing 8 and 12 vol% PEDT with the balance made of PSSH. These compositions were known to give optimal organic light-emitting diode (OLED) performance. PEDT:PSSH:PFI formulations containing also 8 and 12 vol% PEDT were prepared by mixing the purified PEDT:PSSH solution with a commercial PFI dispersion (Nafion perfluorinated resin solution). We used vol% to label these formulations, as this is the key parameter that determines film composition and conductivity percolation. Four formulations were prepared: PEDT-12S, PEDT-8S, PEDT-12F, and PEDT-8F, where the number gives the PEDT vol%, "S" denotes the unmodified formulation (i.e., PEDT:PSSH), and "F" denotes the PFI-modified formulation (i.e., PEDT:PSSH:PFI). **Table 1** gives their detailed compositions. Films were then

Table 1. Compositions of HILs used in this study.

HIL	Weight fraction[a]			Volume fraction[b]		
	PEDT	PSSH	PFI	PEDT	PSSH	PFI
PEDT-12S	0.12	0.88	0.00	0.12	0.88	0.00
PEDT-8S	0.08	0.92	0.00	0.08	0.92	0.00
PEDT-12F	0.11	0.65	0.24	0.12	0.72	0.16
PEDT-8F	0.06	0.37	0.56	0.08	0.48	0.44

[a]Computed from mixing ratio; [b]Computed from weight fractions taking effective density of PEDT and PSSH to be 1.2 g cm^{-3} and PFI to be 1.9 g cm^{-3}.

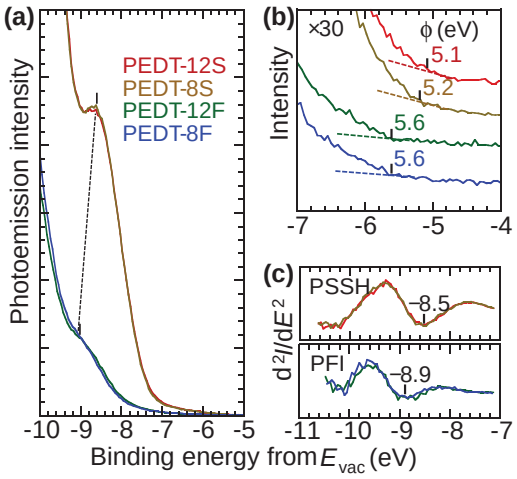

Figure 2. Ultraviolet photoemission spectroscopy of the hole-injection layers. a) UPS spectra showing the valence band region. b) Expanded UPS spectra for the Fermi edge region. c) Second-derivative photoemission spectra showing the rigid shift in the molecular orbital energy on the vacuum energy scale. The spectra in (b) are offset and E_F is marked for clarity. Sample bias, –10.00 V. He I, 21.21 eV. Legend for all parts is as given in (a).

spin-cast and baked in a N_2 glovebox (hotplate 140 °C, 15 min) as in standard practice.

First we show that the high workfunction in the PFI-modified films derives from a surface dipole effect rather than an electrochemical potential shift of their E_F. **Figure 2**a shows the valence band (VB) spectra of the four HILs measured by UPS with He I excitation, and referenced to E_{vac}. Photoemissions from the PEDT sulfur lone pair (S3p) and PSSH phenyl ring molecular orbitals (MOs) overlap together at –8.5 eV,[31] while C-F MOs do not contribute any feature to the displayed region. This composite band is suppressed in the PFI-modified films, suggesting that PSSH is depleted at the film surface. The inelastic mean free path for photoelectrons excited by He I is very short, ≈0.6 nm, and so the spectra are strongly dominated by the topmost surface monolayer. Figure 2b shows the expanded spectra for the E_F region. This region arises solely from PEDT photoemission. The PEDT density-of-states extend up to its E_F, as found elsewhere,[31] characteristic of heavily *p*-doped conducting polymers.[32] The weaker PEDT photoemission from the 8F and 12F films suggests that the PEDT concentration in their topmost 0.6 nm is only about one-half to one-third of that in the unmodified 8S and 12S films.

The ϕ_{vac} is determined in the usual way from photoelectron kinetic energy at the E_F (KE_{Ef}) and at the low-energy cut-off (KE_{LECO}): $\phi_{vac} = KE_{LECO} + h\nu - KE_{Ef}$, where $h\nu$ is the photon energy (21.21 eV).[33] The 8S and 12S HILs have ϕ_{vac} = 5.1 and 5.2 eV, respectively, while both 12F and 8F HILs give 5.6 eV, similar to previous reports.[19,22,34] The workfunctions of PEDT:PSSH:PFI films are thus independent of the PFI ratio over this composition range.

The workfunction in general is given by the sum of electrochemical and surface-dipole contributions: $\phi = \mu + \chi$, where μ is the electrochemical potential of the carriers at E_F and χ is the surface-dipole potential, measured with respect to the Galvani potential. For the family of PEDT:PSSM, it has been established that the dependence of ϕ on M arises solely from μ effects due to the ionic (Madelung) potential set up by the spectator cations and the sulfonate counter-anions.[31] We examined the situation here for the PFI-modified HILs. Figure 2c shows the second derivative spectra of the VB. These can accurately locate the peak position of the sulfur + phenyl MO band. We found this occurs at –8.5 eV in PEDT:PSSH but at –8.9 eV in PEDT:PSSH:PFI, where it is downshifted by 0.4 eV. The widths of second-derivative shapes are identical. These features together with the 0.4 eV downshift of the onset of PEDT photoemission (Figure 2b) confirm that the PEDT and PSSH photoemissions from the PEDT:PSSH:PFI HILs are rigidly downshifted by 0.4 eV. Therefore the increase in their ϕ_{vac} arises entirely from a surface dipole effect. We attribute this dipole to "gauche" and/or twisted —CF_2CF_2—segments producing a negative-outward directed dipole moment.[35]

To probe the deeper composition profile in the surface region of these films, we collected core-level X-ray photoemission spectra at both 90° and 30° emission angles. **Figure 3** shows the C1s, F1s, O1s, and S2p core-level spectra plotted against binding energies (BEs) referenced to E_F and collected at 90° (i.e., perpendicular emission). The $^1/_e$ effective escape depth is ≈2.5 nm at 90° and ≈1.2 nm at 30° for these core levels. The following observations confirm the surface dipole effect and indicate the extent of surface CF_2 enrichment.

First, there is no shift in the BE referenced to E_F for every core level across the series of films despite the 0.4 eV change in workfunction. The C1s photoemissions are found at 284.0 eV (PEDT and PSSH, unresolved) and 291.0 eV (PFI), F1s at 688.2 eV (PFI), O1s at 531.4 eV (PEDT and PSSH), and 534.7 eV (PFI), S2p at 163.6 eV (PEDT) and 168.0 eV (PSSH and PFI). This provides independent confirmation that the rigid bandshift observed in the VB region also applies to the core levels. Thus the increase in ϕ_{vac} indeed arises from a surface dipole that upshifts VL outside the film surface rather than increasing μ which would result in decrease in BEs of all orbitals measured to the E_F.

Second, the PEDT and PSSH C1s core-level emissions are less severely attenuated (only by half) than their VB emissions, in the PFI-modified films. This indicates a strong composition grading at the surface. To quantify the extent of this grading, we evaluated the detected PEDT, PSS, and PFI stoichiometries from the photoemission intensities and inferred their depth profile assuming a monotonic function. The PEDT contribution was resolved from the S2p spectra by curve-fitting using the known shape function of *p*-doped PEDT where the primary $S2p_{3/2}$ BE component lies at 163.6 eV.[36] The PSSH and PFI contributions were then evaluated self-consistently from the detected sulfonate, fluorine, oxygen, hydrocarbon, and fluorocarbon stoichiometries. The evaluated X-ray photoelectron spectroscopy (XPS) compositions, given as volume fractions, are then plotted at the respective electron escape depths, as shown in **Figure 4**.

These results indicate that the PFI-modified films exhibit a marked surface enrichment of PFI at the expense of PSSH. This produces a composition inversion of the matrix polymer in the top 2 nm of the 12F film, and ≈10 nm (extrapolated) of the 8F film. For example, while the bulk of the 12F film comprises 12 vol% PEDT, 72 vol% PSSH, and 16 vol% PFI (Table 1),

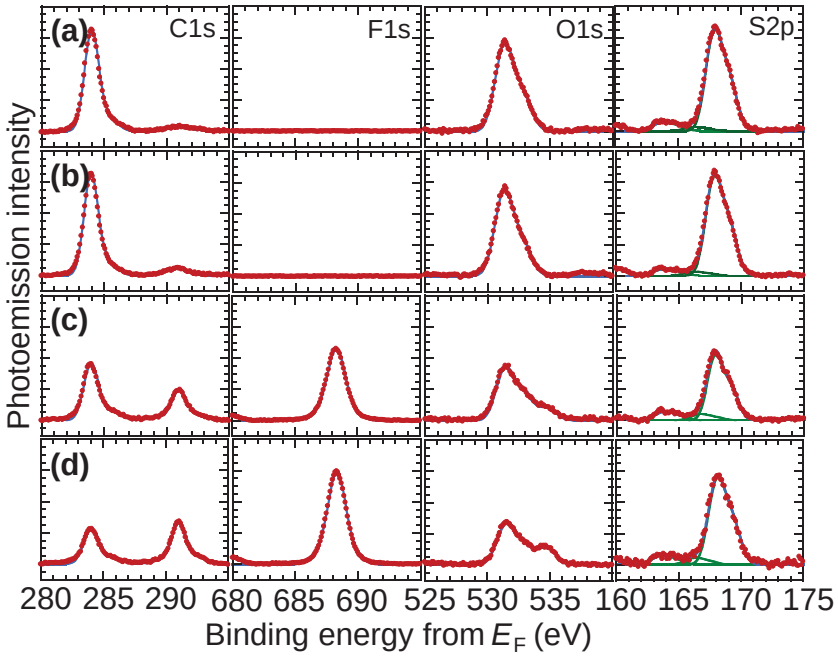

Figure 3. X-ray photoemission spectroscopy of the hole-injection layers. a) PEDT-12S, b) PEDT-8S, c) PEDT-12F, and d) PEDT-8F. Excitation, MgKα 1253.6 eV. Photoemission angle, 90°. Curve-fitting is shown for S2p core level.

the top 2.5 nm comprises on average 6.9 vol% PEDT, 45 vol% PSSH, and 49 vol% PFI, and the topmost 1.2 nm comprises 6.5 vol% PEDT, 23 vol% PSSH, and 70 vol% PFI. The surface CF_2 enrichment results in a large surface energy difference between the modified and unmodified films. Dynamic contact angle measurements with aromatic (p-xylene and *o*-dichlorobenzene) and aliphatic hydrocarbon (decane) solvents showed the advancing contact angles increase from ≈5° on the unmodified films to 45°–69°, depending on solvent, on the PFI-modified films, consistent with measurements on neat PFI film and a PTFE surface (Table S1, Supporting Information). This confirms the presence of a PFI overlayer on the PEDT:PSSH:PFI films.

The PEDT composition profiles however are nearly identical beyond 1 nm or so, between the modified and unmodified films. The general surface depletion of PEDT in PEDT:PSSH films is well-known from XPS[37] and neutron reflectivity[38,39] measurements. It has been shown to be reversible by PEDT electromigration.[36] Yet right at the surface itself, UPS has demonstrated that the PEDT is depleted to 33%–50% in the PFI-modified films compared to pristine films. This confirms the presence of a molecularly thin PFI monolayer overlying the PEDT chains. Moreover the PEDT chains in the subsurface of the modified films are embedded in a PFI-rich matrix rather than a PSSH-rich matrix. The morphology of PEDT in PEDT:PSSH has been a matter of some controversy. Early studies were interpreted in a core–shell model with PEDT encased in PSSH,[40] but later work suggested a network morphology of the PEDT chains, which is consistent with the measured conductivity percolation threshold and possibility of layer-by-layer assembly.[25,41] Since the PEDT depth profile is largely unchanged except at the surface, the PEDT morphology does not appear to have been drastically modified in the PEDT:PSSH:PFI films. Nevertheless the highest-occupied and lowest-unoccupied MOs of PFI are much deeper and shallower, respectively, than those of PSSH. Hence the electron and hole tunneling rates from the embedded PEDT chains in the PFI-modified HIL to the adjoining OSC layer can be expected to be significantly depressed.

Atomic force microscopy reveals all the films have similar nodular surface morphologies. The unmodified films show fine nodules in the 10 nm diameter range with a root-mean-square roughness (R_{rms}) of 1.2–1.6 nm, while the PFI-modified HILs show larger modules of up to a few hundred nanometers in diameter, with R_{rms} increasing with PFI ratio (12F, 2.0 nm; 8F, 4.3 nm; Figure S1, Supporting Information). All the PFI-modified films here are surprisingly smoother than the neat film of PFI which comprises aggregated colloidal particles that do not appear to be well solvated in the aqueous alcohols.[13] The smooth morphology here suggests PSSH help to disperse and compatibilize PFI, suppressing phase segregation beyond the molecular length scale.

We next deduced the energy-level alignment diagrams when these films are used as HILs in contact with a set of model OSCs in simple diode structures and related the diagrams to the measured *JV* characteristics. We chose a set of polymer OSCs spanning a wide I_p range (UPS values): poly(9,9-bis(4-octylphenyl)fluorene-2,7-diyl) (PFOP) as a model for deep-I_p OSC (5.8 eV); poly(9,9′-dioctylfluorene-2,7-diyl-1,4-phenylene-N-(*p*-sec-butylphenyl)amino-1,4-phenylene) (TFB) as a model for medium-I_p OSC (5.5 eV); and 2,5-dialkoxy-substituted poly(*p*-phenylenevinylene) (OC_1C_{10}-PPV) as a model for shallow-I_p OSC (5.1 eV). The chemical structures are given in Figure 1. These polymers are amorphous or nanocrystalline. Thus the molecular packing at their interface with the HILs may not be so sensitive to differences in surface energies. However the modified HILs may lead to a slightly lower-density packing of the OSC at the interface.

We used EA spectroscopy to measure the diode built-in potential V_{bi}[42–45] to obtain the flatband energy-level diagram. The V_{bi} is obtained as the applied dc bias V_{dc} required to null out the quadratic EA Stark effect. We performed these measurements at 30 K to avoid bulk injection and attendant spectral complications. There is often only a small difference (<0.1 eV) in V_{bi} between 30 K and room temperature.[12,46] The V_{bi} is given theoretically by the difference in effective workfunctions of the contacts, $V_{bi} = \phi_{el2} - \phi_{el1}$, where ϕ_{el2} and ϕ_{el1} are the effective workfunctions of the respective electrodes ($\phi_{el2} > \phi_{el1}$).[4] Thus if the ϕ_{el} of one of the contacts is known a priori, the ϕ_{el} of the other contact can be obtained. The electron contact in these diodes was chosen to be Al to provide hole-dominated devices. Although Al is not fully electron-blocking, the injected electron current appears to be small, which does not harm our conclusions. **Figure 5** shows the normalized reflectance spectra $\Delta R/R$, where ΔR is the modulated

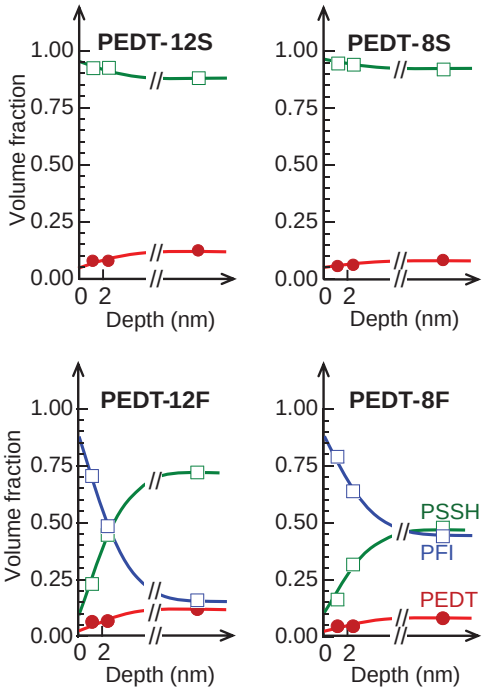

Figure 4. Surface composition profile models for the hole-injection layers. The XPS compositions are plotted at the corresponding electron escape depths, which correspond to the depths where the compositions occur in a linearly graded profile. The bulk compositions are theoretical values computed from the experimental mixing ratio.

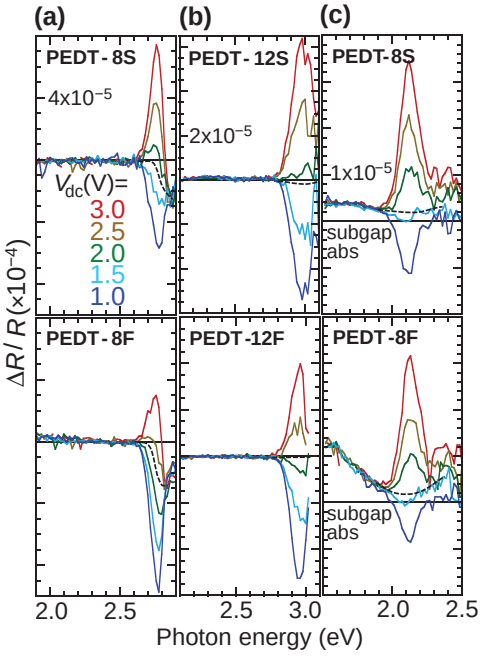

Figure 5. Electromodulated absorption spectra for the hole-dominated diodes with different HILs. a) PFOP, b) TFB, and c) OC_1C_{10}-PPV. Value for the first major tick in each panel column is indicated. Positive value indicates induced absorption in-phase with forward bias half-cycle. Cathode, Al. Temperature, 30 K. Modulation frequency, 535 Hz. Amplitude, 0.5 V rms. Horizontal line, zero. Dashed line, estimated null spectrum. Actual HIL used is as indicated.

root-mean-square reflectance that is in-phase with the forward-bias half-cycle and R is the dc reflectance. **Figure 6** shows the energy-level diagrams deduced for the diodes at 30 K (top) and the measured JV characteristics at 298 K (bottom).

The effective workfunctions of buried metal contacts evaporated onto polymer OSCs have been reliably established previously.[4] Al gives $\phi_{el} = 3.4 \pm 0.1$ eV, which is considerably smaller than its ϕ_{vac}. Since the lowest unoccupied MO edges of PFOP, TFB, and OC_1C_{10}-PPV are all considerably higher than 3.4 eV, the electron contacts are unpinned, and $\phi_{el1} = 3.4$ eV provides a suitable energy reference here for all the energy-level alignment diagrams.

The $\Delta R/R$ EA spectra for PEDT-x/PFOP/Al diodes, where x = 8S and 8F, are shown in Figure 5a. The Stark peak occurs at 2.75 eV, at the $\pi - \pi^*$ absorption edge of PFOP. PFOP does not exhibit β-phase aggregation and hence provides a good model of a nontrapping deep-I_p polymer. The estimated null spectrum shown as a dotted line provides the background for the Stark spectrum. The Stark peak shows polarity inversion at 1.8 (±0.05) V for 8S and 2.25 (±0.05) V for 8F. Hence the effective workfunction of 8S is $\phi_{el} = (3.4 + 1.8)$ eV = 5.2 eV, and of 8F is (3.4 + 2.25) eV = 5.65 eV. These values are in excellent agreement with the respective measured ϕ_{vac} (±0.05 eV). Thus for these HILs in contact with PFOP, $\phi_{el} = \phi_{vac}$, which means the VL are aligned at the contact, and there is no significant additional dipole at the interface. This pair of energy-level diagrams is shown in Figure 6a (top panel). Since the VL offset is negligible (<0.1 eV), there is also negligible δ-hole density at the PFOP interfaces to both these HILs. This is confirmed by the weak or absent subgap polaron absorption in EA spectroscopy (Figure 5a).[10]

The JV characteristics for 8S, 12F, and 8F HILs are practically identical (Figure 6a, bottom panel). The simulated JV characteristic for a hypothetical ohmic hole contact, where the bare potential is set to a realistic value (2.3 V) and the SCLC mobility μ_{SCLC} is assumed to be 2×10^{-4} cm^2 V^{-1} s^{-1}, is shown by the gray curve. The bare potential corresponds to $\phi_{el2} - \phi_{el1}$ for the hypothetical condition of no electrostatic band-bending in the semiconductor[46] arising from the thermal carrier diffusion tail.[47] The experimental curves show a large upshift of ≈1 V at turn-on, indicating a very high initial contact resistance associated with nonohmic hole contacts. Above ≈5 V, the measured JV curves approach ohmic behavior, indicating the hole injection at both types of HILs improves similarly. Thus despite the more favorable ϕ_{el} of the PFI-modified HIL and its lower thermodynamic hole barrier, $\Delta_h = 0.2$ eV, the δ-hole density at the contact remains small and insufficient to turn it ohmic at low voltages.

The EA spectra for PEDT-x/OC_1C_{10}-PPV/Al diodes, where x = 8S and 8F, are shown in Figure 5c. The Stark peak occurs at 2.1 eV, at the OC_1C_{10}-PPV absorption edge. This peak shows polarity inversion at 1.6 (±0.05) V for both HILs. Hence the E_F of both HILs are pinned at 5.0 eV relative to E_{vac}, which is 0.1 eV above the HOMO edge of OC_1C_{10}-PPV (Figure 6c, top panel). The decrease in ϕ_{el} to 5.0 eV corresponds to a VL offset (including electrostatic band bending) of 0.2 and 0.6 eV for the pristine and PFI-modified HIL, respectively. This indicates the presence of a sizeable δ-hole density at the contact, which is confirmed by the modulated subgap absorption intensity below 2.0 eV (Figure 5c). The injected hole density is larger for the modified HIL, since the reduction in its interfacial capacitance

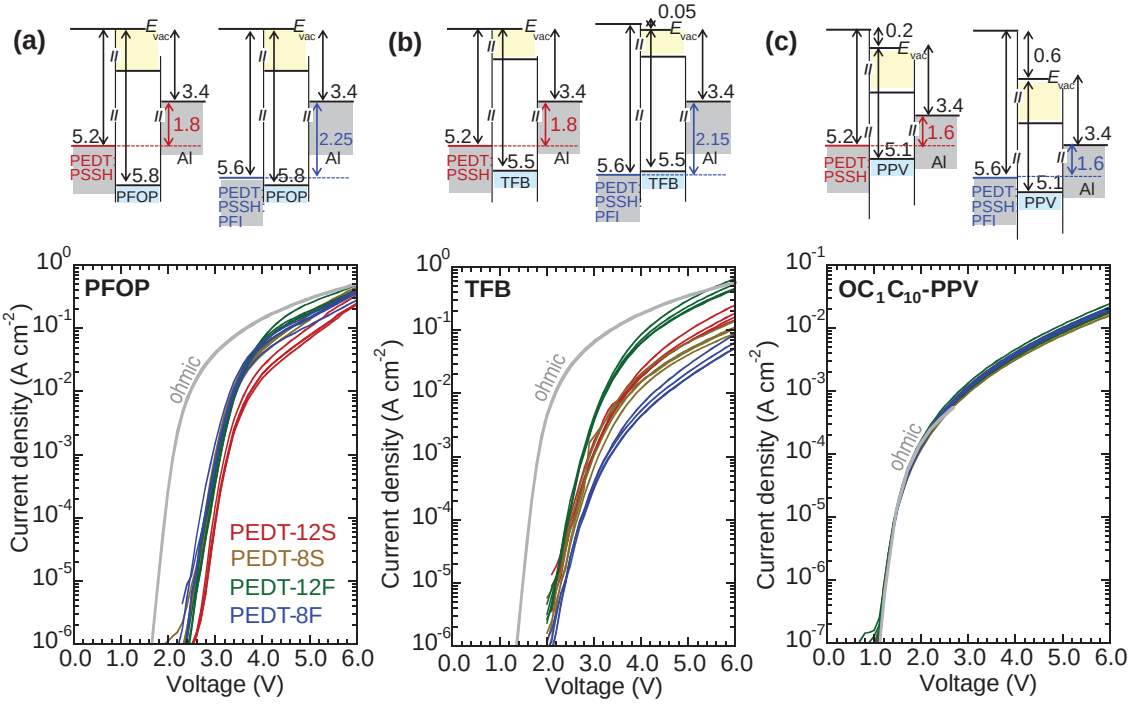

Figure 6. Energy-level alignment diagrams and *JV* characteristics of diodes with the different HILs. a) PFOP, b) TFB, and c) OC_1C_{10}-PPV. Four representative characteristics are shown for each type of diodes. *JV* characteristics are for the second sweep. Gray lines show the simulated ohmic *JV* characteristics, with parameters given in the text. The indicated VL offsets include electrostatic band bending at the contacts, if any.

is expected to be small. This larger hole density would cause a stronger electrostatic band bending in the OSC layer, which implies the E_F is pinned even closer to the HOMO edge of the OSC (<0.1 eV), consistent with the reduction of the polaron polarization energy at this contact.[7–9] The simulated ohmic *JV* characteristics are shown in gray in Figure 6c for a bare potential of 1.6 V, and constant $\mu_{SCLC} = 1.5 \times 10$ cm^2 V^{-1} s^{-1} taken from the work of Blom et al. [48] The measured *JV* characteristics closely follow this simulation up to 3 V, beyond which the carrier-density dependence of μ_{SCLC} needs to be considered.[49] This excellent agreement confirms that both types of HILs give ohmic hole contacts with OC_1C_{10}-PPV. Since the currents are already space-charge-limited, the PFI-modified HIL does not confer an advantage.

The case of a medium-I_p OSC (given by TFB) is expected to be most sensitive to any improvement in hole-injection efficiency. The EA spectra for PEDT-*x*/TFB/Al diodes, where *x* = 12S and 12F, are shown in Figure 5b. The Stark peak occurs at 2.95 eV, at the TFB absorption edge. The PEDT:PSSH/TFB contact resides in the blocking–ohmic borderline regime for hole injection.[12,36] The Stark peak shows polarity inversion at 1.8 (±0.05) V for 12S and 2.15 (±0.05) V for 12F. Hence ϕ_{el} of 12S and 12F in these diodes are 5.2 and 5.55 eV, respectively, thus $\phi_{el} \approx \phi_{vac}$, indicating again VL alignment at the contact with TFB, with a possible small offset of 0.05 eV for the 12F HIL (Figure 6b, top panel). This suggests E_F of the PFI-modified HIL can approach very close to the HOMO edge of TFB. The apparent crossing of the conventionally defined edge may be attributed to an error in the location of the edge due to a reduction of the polaron energy in contact with the HIL. *JV* characteristics indicate the PFI-modified HILs do not consistently nor significantly improve the hole current density (Figure 6b). The simulated ohmic *JV* characteristics are shown as a gray line, for a bare potential of 2.0 V, and $\mu_{SCLC} = 2 \times 10^{-4}$ cm^2 V^{-1} s^{-1} taken from the work of Blakesley et al.[50] The measured *JV* characteristics clearly fall well below the ohmic characteristic at turn-on (i.e., very high contact resistance there), approaching it only at high drive voltages.

Therefore it is clear that the PFI-modified HILs are not as effective in injecting holes into the OSC as might have been expected from simple thermodynamic considerations of the reduction in the Δ_h. Although the modified HILs may have induced a slightly different molecular organization of the polymer OSC at the contact, a consistent picture has emerged that suggests the dominant effect is related to the energetics and kinetics of charge transfer. The measurements have revealed a large contact resistance particularly at turn-on, consistent with the presence of a PFI overlayer in the HIL; and a low equilibrium density of holes at the semiconductor contact, attributed to a lower interfacial capacitance and loss of polaron stabilization energy due to the lower dielectric constant. These two factors together mitigate the benefits of having an ultrahigh workfunction. Thus workfunction alone is not a sufficient condition for ohmic contacts. The contact needs to be able to inject the required carrier density into the semiconductor interface, which is rather obvious, but often neglected in the literature.

Finally we outline the case of a double-carrier OLED. A film of a model light-emitting polymer OSC, poly(9,9-dioctylfluorene-2,7-diyl-*alt*-benzo-2,1,3-thiadiazole-4,7-diyl) (F8BT, I_p = 5.9 eV), is fabricated on 8S and 8F as HIL, and evaporated with

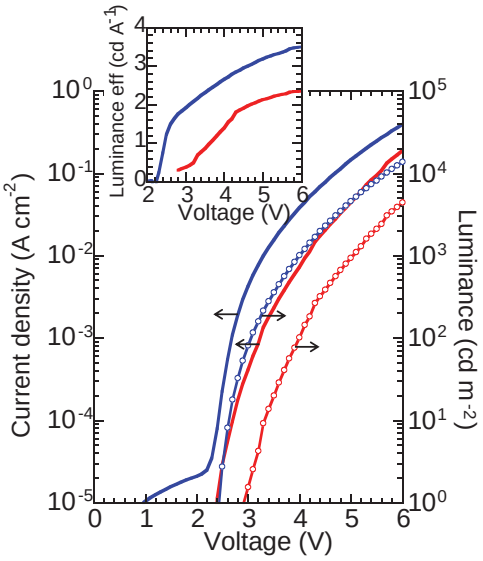

Figure 7. *JVL* characteristics of double-carrier light-emitting diodes with F8BT as light-emitting polymer. HIL = PEDT-8S (red), PEDT-8F (blue). The inset shows the voltage dependence of luminance efficiency. Emission spectrum center wavelength, 550 nm.

Al or Ca as electron contact. The *JV* curves of diodes with Ca electron contact and the two HILs are given in **Figure 7**. The double-carrier diode with Ca contact does exhibit a significant enhancement in both current density and luminescence efficiency, particularly just above turn-on, while the hole-dominated diode (Al electron contact) does not give any enhanced current density (not shown). This behavior suggests that hole injection is enhanced in the presence of the opposite carriers, which is reminiscent of the use of an ultrathin self-assembled polyelectrolyte monolayer[25] or TFB layer[51] to block electron leakage in devices. Therefore we speculate that the improvement in this and other double-carrier diodes reported in the literature arises from electron blocking, rather than the formation of true ohmic hole contact which has been ruled out here.

In summary, the ultrahigh workfunctions of PEDT:PSSH:PFI blends are due to the development of a dipolar surface layer associated with surface segregation of PFI chains. This is confirmed by (i) the rigid VB shift observed in UPS, (ii) the suppression of PEDT and PSS photoemission, and (iii) the closer approach of the Fermi level of these HILs to the HOMO edge of a set of polymer OSCs observed in diode built-in potential measurements. Despite their higher workfunctions of 5.6 eV, their hole contacts to OSCs with ionization potentials deeper than ≈5.2 eV remain nonohmic. This is attributed to (i) interfacial resistance to hole-injection and (ii) lower equilibrium hole densities at the semiconductor side of the contact, as evidenced by subgap charge modulation measurements. As a consequence, the contact is unable to provide the required carrier density to reach ohmic behavior. Thus workfunction matching through the use of an insulating dipolar layer is not efficient for providing ohmic contacts. A different set of approaches is required to impose the desired large charge-carrier density at the semiconductor interface at relatively shallow pinning depths.

3. Experimental Section

Materials: PEDT:PSSH was obtained from HC Starck (Baytron P, Leverkusen, Germany; now Clevios P VP Al 4083, from Heraeus Precious Metals GmbH) as a 1:6 w/w (weight/weight) material corresponding to 14 vol% PEDT dispersed in 86 vol% PSSH. PSSH (Mw = 70 k) was obtained from Scientific Polymer Products (N.Y.) and dissolved in Millipore water. PFI was obtained from Sigma Aldrich (Nafion perfluorinated resin solution) as a 5 wt% dispersion in a mixed solvent of 45 vol% water and 55 vol% lower aliphatic alcohols. The equivalent weight is 1100.

UPS and XPS: Ultraviolet photoemission spectroscopy (UPS) was performed using He I radiation (21.21 eV) in a VG ESCALab Mk-II spectrometer operated at a base pressure of 1×10^{-9} mbar. A sample bias of –10.00 V was applied to collect all the photoemission. 50 nm thick HIL films were spin-cast on Au-coated Si substrates and baked at 140 °C (hotplate) for 10 min in the N_2 glovebox (pH2O, pO2 < 1 ppm). XPS was performed on the same films as the UPS, after UPS, using MgKα X-ray (1253.6 eV), respectively, on VG ESCALab Mk-II spectrometer, at 30° and 90° acceptance angles (with respect to the analyzer). All spectra have been corrected using linear backgrounds. The integration of these spectra after correction with the empirical sensitivity factors provides the atomic stoichiometry determined by XPS. Quantification error is expected to be ±10%.

Device Fabrication and Characterization: Hole-dominated devices were fabricated by spin coating HIL solutions, in ambient, on standard clean 1 (SC1) cleaned indium tin oxide (ITO) substrates to attain a 50 nm film. The solutions were prefiltered through a 0.45 µm nylon syringe filter. The films were annealed at 140 °C (hotplate) for 10 min in glovebox. 10 mg mL^{-1} OC_1C_{10}-PPV, 15 mg mL^{-1} TFB, and 15 mg mL^{-1} PFOP solutions in toluene were prepared from polymers obtained from Cambridge Display Technology. The polymer OSC films were spin-coated over the HILs in the glovebox to give 120 nm thick films and annealed at 120 °C (hotplate) for 10 min in glovebox. A 120 nm thick aluminum film was then thermally evaporated through a shadow mask at a base pressure of 10^{-7} Torr to give the cathode for eight 4.3 mm^2 pixels on each substrate. The current–voltage characteristics were collected on a probe station in the glovebox using a Keithley 4200 semiconductor parameter analyzer. Film thicknesses were measured by a profilometer (Tencor P2).

Electroabsorption Spectroscopy: Electroabsorption (EA) spectroscopy measurements of the diodes were performed at 30 K in a closed-cycle He cryostat (Janis APD HC-2). The pressure inside the chamber was maintained at 10^{-6} mbar. A sinusoidal drive voltage superposed on the selected dc bias was injected into the diode. Monochromatic light was incident through the glass substrate at 45°, and its reflection of the cathode collected by mirror optics onto a photodiode. The voltage output was demodulated by a lock-in amplifier phase locked to the ac to give the change in absorbance for a range of wavelength.

Current Density–Voltage (JV) Characteristics Simulation: The *JV* characteristics were simulated using standard diffusion–drift equations assuming a hole-dominated current, a diffusion slope $\frac{\partial \ln J}{\partial V} = \frac{e}{nkT}$, with $n = 2$, and a contact carrier density of 2×10^{17} cm^{-3}. The integrated contact carrier density is $\approx 1 \times 10^{11}$ cm^{-2}, as suggested experimentally.[4,10]

Supporting Information

Supporting Information is available from the Wiley Online Library or from the author.

Acknowledgements

P.F.D. and Y.M.L. performed part of the work as an Advanced Research Project administered by the NUS High School of Math and Science. B.N.N.T and N.S.R. performed part of the work as a Young Defense Science Project administered by Defense Science & Technology Agency, Singapore. This research was partially supported by the

National Research Foundation, Prime Minister's Office, Singapore under its Competitive Research Programme (CRP Award No. NRF-CRP 11-2012-03).

Received: February 27, 2015
Revised: June 24, 2015
Published online: August 4, 2015

[1] G. G. Malliaras, J. C. Scott, *J. Appl. Phys.* **1998**, *83*, 5399.
[2] Y. Shen, A. R. Hosseini, M. H. Wong, G. G. Malliaras, *Chem. Phys. Chem.* **2004**, *5*, 16.
[3] H. T. Nicolai, G. A. H. Wetzelaer, M. Kuik, A. J. Kronemeijer, B. de Boer, P. W. M. Blom, *Appl. Phys. Lett.* **2010**, *96*, 172107.
[4] M. Zhou, R. Q. Png, S. H. Khong, S. Sivaramakrishnan, L. H. Zhao, L. L. Chua, R. H. Friend, P. K. H. Ho, *Appl. Phys. Lett.* **2012**, *101*, 013501.
[5] S. Braun, W. R. Salaneck, M. Fahlman, *Adv. Mater.* **2009**, *21*, 1.
[6] J. H. Hwang, A. Wan, A. Kahn, *Mater. Sci. Eng. R* **2009**, *64*, 1.
[7] L. H. Zhao, R. Q. Png, C. C. H. Chiam, H. Guo, J. M. Zhuo, L. L. Chua, A. T. S. Wee, P. K. H. Ho, *Appl. Phys. Lett.* **2012**, *101*, 053304.
[8] E. V. Tsiper, Z. G. Soos, W. Gao, A. Kahn, *Chem. Phys. Lett.* **2002**, *360*, 47.
[9] N. Koch, G. Heimel, J. S. Wu, E. Zojer, R. L. Johnson, J. L. Bredas, K. Mullen, J. P. Rabe, *Chem. Phys. Lett.* **2005**, *413*, 390.
[10] M. Zhou, L. L. Chua, R. Q. Png, C. K. Yong, S. Sivaramakrishnan, P. J. Chia, A. T. S. Wee, R. H. Friend, P. K. H. Ho, *Phys. Rev. Lett.* **2009**, *103*, 0366011.
[11] B. K. Crone, P. S. Davids, I. H. Campbell, D. L. Smith, *J. Appl. Phys.* **1998**, *84*, 833.
[12] M. Zhou, R. Q. Png, S. Sivaramakrishnan, P. J. Chia, C. K. Yong, L. L. Chua, P. K. H. Ho, *Appl. Phys. Lett.* **2010**, *97*, 113505.
[13] K. A. Mauritz, R. B. Moore, *Chem. Rev.* **2004**, *104*, 4535.
[14] L. B. Groenendaal, F. Jonas, D. Freitag, H. Pielartzik, J. R. Reynolds, *Adv. Mater.* **2000**, *12*, 481.
[15] S. Kirchmeyer, K. Reuter, *J. Mater. Chem.* **2005**, *15*, 2077.
[16] C. T. Brown, V. Seshadri, M. Mathai, B. Woodworth, D. Laird, *SID Int. Sym. Dig. Tec.* **2010**, *41*, 461.
[17] D. Belaineh, R. Q. Png, C. L. McGuiness, M. Mathai, V. Seshadri, P. K. H. Ho, *Chem. Mater.* **2014**, *26*, 4724.
[18] C. Tengstedt, W. Osikowicz, W. R. Salaneck, I. D. Parker, C. H. Hsu, M. Fahlman, *Appl. Phys. Lett.* **2006**, *88*, 053502.
[19] T. W. Lee, O. Kwon, M. G. Kim, S. H. Park, J. Chung, S. Y. Kim, Y. Chung, J. Y. Park, E. Han, D. H. Huh, *Appl. Phys. Lett.* **2005**, *87*, 231106.
[20] T. W. Lee, Y. Chung, O. Kwon, J. J. Park, *Adv. Funct. Mater.* **2007**, *17*, 390.
[21] J. Park, Y. Kwon, T. W. Lee, *Macromol. Rapid Commun.* **2007**, *28*, 1366.
[22] S. A. Mauger, J. Li, O. T. Ozmen, A. Y. Yang, S. Friedrich, M. D. Rail, L. A. Berben, A. J. Moulé, *J. Mater. Chem. C* **2014**, *2*, 115.
[23] S. Sivaramakrishnan, M. Zhou, A. C. Kumar, Z. L. Chen, R. Q. Png, L. L. Chua, P. K. H. Ho, *Appl. Phys. Lett.* **2009**, *95*, 213303.
[24] P. K. H. Ho, M. Granström, R. H. Friend, N. C. Greenham, *Adv. Mater.* **1998**, *10*, 769.
[25] P. K. H. Ho, J. S. Kim, J. H. Burroughes, H. Becker, S. F. Y. Li, T. M. Brown, F. Cacialli, R. H. Friend, *Nature* **2000**, *404*, 481.
[26] M. L. Sushko, A. L. Shluger, *Adv. Mater.* **2009**, *21*, 1111.
[27] W. Osikowicz, X. Crispin, C. Tengstedt, L. Lindell, T. Kugler, W. R. Salaneck, *Appl. Phys. Lett.* **2004**, *85*, 1616.
[28] P. J. Hotchkiss, H. Li, P. B. Paramonov, S. A. Paniagua, S. C. Jones, N. R. Armstrong, J. L. Brédas, S. R. Marder, *Adv. Mater.* **2009**, *21*, 4496.
[29] Y. Zhou, C. Fuentes-Hernandez, J. Shim, J. Meyer, A. J. Giordano, H. Li, P. Winget, T. Papadopoulos, H. Cheun, J. Kim, M. Fenoll, A. Dindar, W. Haske, E. Najafabadi, T. M. Khan, H. Sojoudi, S. Barlow, S. Graham, J. L. Brédas, S. R. Marder, A. Kahn, B. Kippelen, *Science* **2012**, *336*, 327.
[30] P. J. Chia, L. L. Chua, S. Sivaramakrishnan, J. M. Zhuo, L. H. Zhao, W. S. Sim, Y. C. Yeo, P. K. H. Ho, *Adv. Mater.* **2007**, *19*, 4202.
[31] P. J. Chia, S. Sivaramakrishnan, M. Zhou, R. Q. Png, L. L. Chua, R. H. Friend, P. K. H. Ho, *Phys. Rev. Lett.* **2009**, *102*, 0966021.
[32] M. Lögdlund, R. Lazzaroni, S. Stafström, W. R. Salaneck, J. L. Brédas, *Phys. Rev. Lett.* **1989**, *63*, 1841.
[33] N. Koch, C. Chan, A. Kahn, J. Schwartz, *Phys. Rev. B* **2003**, *67*, 1953301.
[34] J. X. Tang, C. S. Lee, S. T. Lee, *J. Appl. Phys.* **2007**, *101*, 0645041.
[35] T. Hasegawa, T. Shimoaka, N. Shioya, K. Morita, M. Sonoyama, T. Takagi, T. Kanamori, *ChemPlusChem* **2014**, *79*, 1421.
[36] R. Q. Png, P. J. Chia, S. Sivaramakrishnan, L. Y. Wong, M. Zhou, L. L. Chua, P. K. H. Ho, *Appl. Phys. Lett.* **2007**, *91*, 013511.
[37] G. Greczynski, T. Kugler, M. Keil, W. Osikowicz, M. Fahlman, W. R. Salaneck, *J. Electron Spectrosc. Relat. Phenom.* **2001**, *121*, 1.
[38] P. C. Jukes, S. J. Martin, A. M. Higgins, M. Geoghegan, R. A. L. Jones, S. Langridge, A. Wehrum, S. Kirchmeyer, *Adv. Mater.* **2004**, *16*, 807.
[39] S. J. Martin, R. A. L. Jones, M. Geoghegan, A. M. Higgins, I. Grizzi, J. J. M. Halls, S. Kirchmeyer, R. M. Dalgliesh, *Phys. Rev. B* **2005**, *71*, 081308.
[40] X. Crispin, S. Marciniak, W. Osikowicz, G. Zotti, A. W. Denier van der Gon, F. Louwet, M. Fahlman, L. Groenendaal, F. De Schryver, W. R. Salaneck, *J. Polym. Sci. B: Polym. Phys.* **2003**, *41*, 2561.
[41] A. M. Nardes, M. Kemerink, R. A. J. Janssen, J. A. M. Bastiaansen, N. M. M. Kiggen, B. M. W. Langeveld, A. J. J. M. van Breemen, M. M. de Kok, *Adv. Mater.* **2007**, *19*, 1196.
[42] I. H. Campbell, M. D. Joswick, I. D. Parker, *Appl. Phys. Lett.* **1995**, *67*, 3171.
[43] I. H. Campbell, J. P. Ferraris, T. W. Hagler, M. D. Joswick, I. D. Parker, D. L. Smith, *Polymer. Adv. Tech.* **1997**, *8*, 417.
[44] T. M. Brown, J. S. Kim, R. H. Friend, F. Cacialli, *Appl. Phys. Lett.* **1999**, *75*, 1679.
[45] V. Bodrozic, T. M. Brown, S. Mian, D. Caruana, M. Roberts, N. Phillips, J. J. Halls, I. Grizzi, J. H. Burroughes, F. Cacialli, *Adv. Mater.* **2008**, *20*, 2410.
[46] B. Liu, R. Q. Png, J. K. Tan, P. K. H. Ho, *Adv. Energy Mater.* **2014**, *4*, 1200972.
[47] W. F. Pasveer, J. Cottaar, C. Tanase, R. Coehoorn, P. A. Bobbert, P. W. M. Blom, D. M. de Leeuw, M. A. J. Michels, *Phys. Rev. Lett.* **2005**, *94*, 206601.
[48] P. W. M. Blom, M. C. J. M. Vissenberg, *Phys. Rev. Lett.* **1998**, *80*, 3819.
[49] C. Tanase, E. J. Meijer, P. W. M. Blom, de D. M. Leeuw, *Phys. Rev. Lett.* **2003**, *91*, 216601.
[50] J. C. Blakesley, F. A. Castro, W. Kylberg, G. F. A. Dibb, C. Arantes, R. Valaski, M. Cremona, J. S. Kim, J. S. Kim, *Org. Electron.* **2014**, *15*, 1263.
[51] R. Q. Png, P. J. Chia, J. C. Tang, B. Liu, S. Sivaramakrishnan, M. Zhou, S. H. Khong, H. S. O. Chan, J. H. Burroughes, L. L. Chua, R. H. Friend, P. K. H. Ho, *Nature Mater.* **2010**, *9*, 152.